Title:

Sequence-nonspecific stabilization of transmembrane helical peptide dimer in lipid raft-like bilayers in atomistic simulations. I. Dimerization free energy and impact of lipid-peptide potential energy

Authors:

Manami Nishizawa and Kazuhisa Nishizawa*

*Corresponding author: **K. Nishizawa** (email: kazunet@med.teikyo-u.ac.jp)

Teikyo University School of Medical Technology,

Kaga, Itabashi, Tokyo, 173-8605 Japan

This paper has been accepted as

Journal title:

Ann Biomed Res

Vol:

1(1)

Page:

105

URL:

http://escires.com/articles/ABR-1-105.pdf

Key words: electrostatic interaction, Lennard-Jones interaction, lipid raft, solvation, membrane protein clustering, lateral interaction

Abstract

Dimerization/oligomerization of transmembrane (TM) helical domains of membrane proteins is considered important in regulation of cell signaling. How cholesterol and saturated fatty acid (FA) chains in membrane phospholipids influence the TM domain interaction in a sequence-nonspecific manner is poorly understood. Here we performed 280μs united-atom and 32μs all-atom molecular dynamic simulations to measure the free energy of dimerization of model peptides with simple amino acid sequences ($(Ile)_{21}$ and $I(VI)_{10}$). Consistent with experiments, lipid bilayers with high concentrations of saturated FA and cholesterol stabilized the dimeric state of the peptides. Potential energy decomposition analysis showed a consistent trend that, for both peptides, both van der Waals and electrostatic interactions between lipids and peptides contribute to monomer-dimer equilibrium alteration dependent on bilayer lipid composition. Intriguingly, despite the lack of polar/charged amino acid residues in the peptides used, our results demonstrated the importance of interactions between lipid head group atoms and peptides backbone atoms. Our results also suggest usefulness of atomistic simulations in studying the acyl chain order-associated sequence-nonspecific TM helix dimer stabilization in raft-like bilayers.

1. Introduction

Recent studies on receptor signaling have elucidated that transmembrane (TM) domain associations are utilized for regulation of activities of single–pass membrane receptor proteins [1]. In early models, the signaling of cytokine receptors and receptor tyrosine kinases was postulated to be an equilibrium between 'inactive monomers' and 'ligand-bound active dimers' [2,3]. However, more recent studies have postulated a 'pre-formed dimer' model, in which not only the presence of inactive dimers but also the subsequent ligand-induced structural changes are important for activation of many receptors [1,4]. For example, 30 to 60% of molecules of human vascular endothelial growth factor receptor (VEGFR)-2, have been shown to exist in the dimeric form in the absence of ligand, and the ligand binding induces a conformational change in the TM domain dimer structure causing increased phosphorylation [1]. Existence of at least two distinct active configurations corresponding to two different ligands has been suggested for human fibroblast growth factor receptor (FGFR)-3 [5]. Although diverse modalities of achieving active states are used by different single-span receptor proteins [4], TM helices dimerization in general plays a permissive role, which is required for further activation

events.

The lipid environment is considered to have significant influences on the monomer-dimer equilibrium of membrane proteins [6]. For example, using a system of palmitoyloleoylphosphatidylcholine (POPC) liposomes containing syntaxin-1A, a single-span TM protein important for neuronal membrane fusion, Murray and Tamm showed that an increase of cholesterol content from 0 to 40 % dramatically induced self-association and clustering of syntaxin-1A [7]. In some other cases, oligomerization of membrane receptors is associated with their translocation to particular membrane microdomains. For example, lutenizing hormone (LH) receptors unbound to ligands are located in non-rafts and, after ligand binding, translocate into lipid rafts [8]. In the case of toll-like receptor (TLR)4, a key player in innate immunity, dimerization and recruitment into lipid rafts are likely to be two events coupled to each other and important for TLR4 activation [9]. Themodynamically, these suggest that the lipid compositions of lipid rafts can stabilize the dimeric state of receptors compared to those of non-raft microdomains [10]. However, it has not been straightforward to draw universal principle governing dynamics, as numerous specific and nonspecific peptide-peptide and lipid-peptide interactions are modulating TM helix association [6,11].

Besides specific interactions between certain lipid species and TM helical peptides, less-specific contacts of lipids with peptides have also been suggested have influences on peptides dynamics [12,13]. Analyses using simple sequences and lipid bilayers with well-defined components have been utilized to characterize sequence-nonspecific effects of lipids on TM helix association. However, only a limited number of studies have focused on sequence-nonspecific effects of cholesterol and saturated fatty acids (FAs). Yano et al showed that, when cholesterol concentration increased from 0 to 30%, dimerization of $(AALALAA)_3$ helical peptide in a POPC membrane was stabilized; the dimerization free energy decreased from −13.2 to −22.6 kJ/mol [14]. The latter study used a peptide with no flanking polar/charged amino acid residues, allowing analyses less confounded by interactions between lipid head group and polar/charged amino acids residues. However, atomic details of sequence-nonspecific effects of lipids on TM helical peptide dimerization/multimerization remain elusive. It is widely accepted that cholesterol reduces trans-gauche isomerizations of the neighboring lipid acyl chains [15], and it is known in some settings that cholesterol and saturated FAs can stabilize dimeric/oligomeric forms of TM helical peptides in a sequence-nonspecific fashion [10,11,14], yet how such lipid ordering modulates TM dimerization remains unclear. Schneider and coworkers showed that in addition to thickness, acyl chain ordering is a key factor stabilizing dimer of glycophorin A (GpA) TM peptide [11]. However, how

universal the dimer-stabilizing effect of cholesterol is not clear [16].

In our recent molecular dynamics (MD) simulations, a bilayer with a high acyl chain order (i.e., a 1:1:1 POPC/dipalmitoylphosphatidylcholine (DPPC)/cholesterol bilayer) exhibited a dimeric state-stabilizing effect for a poly-Ile model peptide ($(Ile)_{21}$), compared with a dioleoylphosphatidylcholine (DOPC) bilayer [10]. This was technically encouraging as simulations using an united-atom (UA) parameters can yield reproducible results at a reasonable level of computational cost. We further observed that desolvation of peptides from lipids upon peptide dimerization in the 1:1:1 bilayer leads to a reduced amount of the energy cost compared to the case in the DOPC bilayer, suggesting that improved solvation (contacts) of dimeric peptides by lipids is important for the overstabilization of the dimer in the raft-like bilayer [10]. However, in that report the analysis was limited in terms of membrane composition, inter-peptide distance and the impact of the electrostatic potential energy compared to that of the Lennard-Jones (LJ) energy. In this report and our upcoming sister paper, we widen the analysis regarding the range of the inter-peptide distance, the types of force fields (UA vs all-atom (AA)), the membrane composition, the model peptide and the energy component (the electrostatic energy as well as the LJ energy). In the sister paper, we discuss the structural features in lipid-peptide contacts associated with the stabilization of the peptides dimer in the raft-like bilayers [17].

2. Methods

2.1 *System Description*

All MD simulations were carried out with the Gromacs suite version 4.5.4 [18]. The UA force-field (FF) GROMOS^{53A6} was downloaded from the automated FF topology builder (ATB) website [19] and the Gromacs-implemented version (implemented the Gromacs) of DOPC, POPC, DPPC and cholesterol were also utilized. Simple-point charge water [20] was used with GROMOS^{53A6}. The initial coordinates for lipid bilayers and peptides were prepared by modifying our recent files [21,22]. For AA simulations, Charmm36 FF for peptides and lipids [23,24] and transferable intermolecular potential 3P (TIP3P) water topology files were used as provided by Gromacs.

Uncharged CH_3CO and NH_2 groups were used to cap the N- and the C-termini, respectively. The LJ interactions were treated with a shift function from 0.8 to 1.3 nm. For the long-range electrostatic energy, the particle-mesh Ewald algorithm [25] was used with a real-space cutoff of 1.4 nm and the minimal grid size of 0.12 nm. Integration time step of 2.5fs was used. To control the temperature at 323 K, the Berendsen thermostat

was used [26]. The semi-isotropic pressure coupling at 1 bar with Berendsen algorithm was used as in our recent report [21]. The bond lengths of lipids and proteins were restrained with LINCS for GROMOS systems [27] and with SETTLE for Charmm systems [28].

2.2 *Potential of mean force computation*

The free energy of dimerization was measured using the umbrella sampling method based on the pull-code module of Gromacs, and the output files were merged with the weighted histogram method (WHAM) [28]. For the umbrella sampling, a harmonic potential with a force constant of 3000 kJ/mol/nm^2 was imposed on the distance (r) between the centers of mass (com) of the helical peptides. Eight independent umbrella analysis sets were performed, each consisting of runs with ten different target interhelical distances (r) ranging from 1.1 to 2.0 nm with a spacing of 0.1 nm for the GROMOS systems (Table 1). For the Charmm sets the r range was limited to 1.3, 1.4, 1.5 and 1.6 nm. To prepare initial structures, two peptides were inserted in an antiparallel orientation into the equilibrated bilayers and overlapping lipids were manually moved. To reduce the influence of initial structures, all the eight initial structures were independently prepared for each r. For all systems (Table 1), a 100-ns equilibration run was performed before the 500-ns production run. After using the WHAM method to compute the potential of mean force (PMF) profile $G^{PMF}(r)$, K_a, the association constant defined as $K_a = [\int \pi r g(r)\, dr]/P_m$ was computed, where integration runs from 0 to R_c, with R_c being the upper limit of r defining the dimeric state. Of note, K_a corresponds to the time length during which the two peptides are dimerized relative to that during which they are in monomers. g(r) is the two-dimensional radial distribution function (rdf) profile derived from $G^{PMF}(r)$ by compensating the Boltzmann factor $\exp(-\beta G^{PMF}(r))$ with respect to the r-dependent increase in available phase space ('entropic force'). P_m is the normalization factor given as $P_m = [v/\{\pi(R_{max}^2 - R_c^2)\}] * [\int \pi r g(r)\, dr]$, where v is the bilayer area available to a peptide monomer at the standard concentration and the integration runs from R_c to R_{max}. Of note, P_m corresponds to a 'normalized v', in other words, v weighted by the time length during which the two peptides are in monomers estimated by the integration. Thus obtained K_a was used to derive the dimerization free energy ΔG^{dim} for helical peptides based on $\Delta G^{dim} = -RT \ln K_a$. In this study, R_c was set at 1.6 nm and v at 1.66 nm^2. On 40 Intel four-core 2.8 GHz CPUs, a DOPC set (#1 of Table 1) of PMF analysis (500 ns/window, n = 8) took ~60 days, while the computation time grew ~1.5-fold for a 1:1:1 bilayer run.

2.3 *Potential energy decomposition analysis*

The three potential energy terms mainly governing the monomer-dimer equilibrium of the peptides, that is, the peptide-peptide ($V_{pept\text{-}pept}$), lipid-lipid ($V_{lipid\text{-}lipid}$), and peptide-lipid ($V_{lipid\text{-}pept}$) potential energy, were obtained from the simulations performed for the umbrella sampling. These were further decomposed into the LJ potential energy terms $V^{LJ}_{pept\text{-}pept}$, $V^{LJ}_{lipid\text{-}pept}$ and $V^{LJ}_{lipid\text{-}lipid}$ and the electrostatic energy terms $V^{Coul}_{pept\text{-}pept}$, $V^{Coul}_{lipid\text{-}pept}$ and $V^{Coul}_{lipid\text{-}lipid}$. It is important to recognize that decomposition analysis of this study cannot be taken as an accurate decomposition of thermodynamics, as the effects of the umbrella harmonic potential and the pressure-volume term were ignored as discussed in Castillo et al [30]. Moreover, if the nonlinearity between r and potential energy terms (such as $V^{LJ}_{lipid\text{-}pept}$ (r)) is large, the use of the ensemble average of each should cause bias. So, the potential energy analysis in this study was conducted for an approximate illustration of the relationship between interhelical distance r and each components including $V^{Coul}_{lipid\text{-}pept}$ and $V^{LJ}_{lipid\text{-}pept,}$ rather than an accurate decomposition of the enthalpy component of free energy profile.

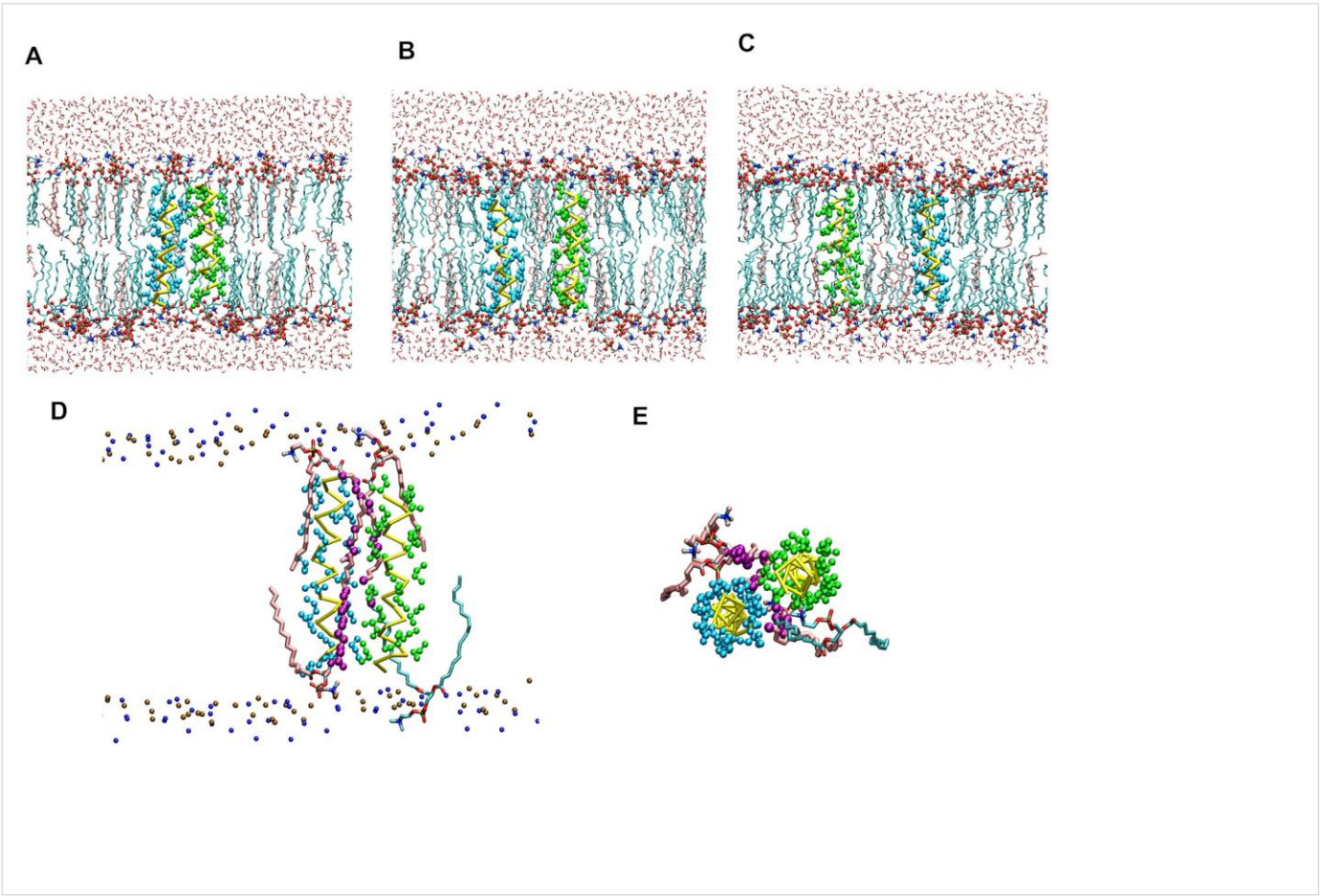

Figure 1
Representative snapshots of PMF simulations of the poly-Ile ($(Ile)_{21}$) model peptide. (A) The GROMOS 1:1:1 POPC/DPPC/cholesterol system (#2 Gr-Ile_{21}-1-1-1 set of Table 1) with interhelical distance r = 1.3 nm. Representation scheme: cyan licorice, lipid acyl chains; red and blue spheres, phospholipid head group oxygen and nitrogen atoms; small balls and sticks, water atoms; yellow bars, peptide backbone trace; green and cyan spheres, Ile side chains. Only lipid molecules located within a 2.0-nm-thick slice are shown. (B) The same as (A) but a simulation run with r = 2.0 nm. (C) The same as (A) but a simulation run with r = 2.5 nm. (D) A timeframe of the Gr-Ile_{21}-1-1-1 set (r = 1.3 nm) that showed dually contacting phospholipids (pink licorice representation). The acyl chain atoms showing dual contacts are highlighted in purple spheres. Phospholipid nitrogen and phosphorus atoms are also shown as in (A). (E) A view from the bottom of the structure presented in (D) but only the lipids with dual contacts are shown for clarity.

3. Results and Discussions

3.1 Increases in cholesterol and saturated FA-chains in phospholipid bilayers cause stabilization of dimeric state of model helical peptides

To examine the effects of cholesterol and saturated FA chains in phospholipid bilayer membranes on the dimerization of transmembrane helical peptides, the dimerization free energies were measured based on the PMF profiles computed for the systems of model peptides/bilayer listed in Table 1. Figure 1A,B,C show representative snapshots from the 1:1:1 POPC/DPPC/cholesterol bilayer/$(Ile)_{21}$ system (#2 of Table 1). The $-S_{CD}$ values that represent the acyl chain order parameters of the peptide-containing bilayers are shown in Figure 2. As expected, the 1:1:1 and 2:1:1 bilayers (#2 and 3, respectively) showed higher order parameters (Figure 2A) compared to the POPC (#4) and the 3:1 POPC/cholesterol (#5) bilayers (Figure 2B), which were in turn relatively high compared to the DOPC bilayer (Figure 2A). The Charmm DOPC and 1:1:1 systems showed acyl chain orders similar to, but slightly lower than, the corresponding GROMOS systems

(Figure 2C). We henceforth refer to the 1:1:1 and 2:1:1 bilayers (i.e., the bilayers of #2, 3, 7, and 9) as the raft-like bilayers.

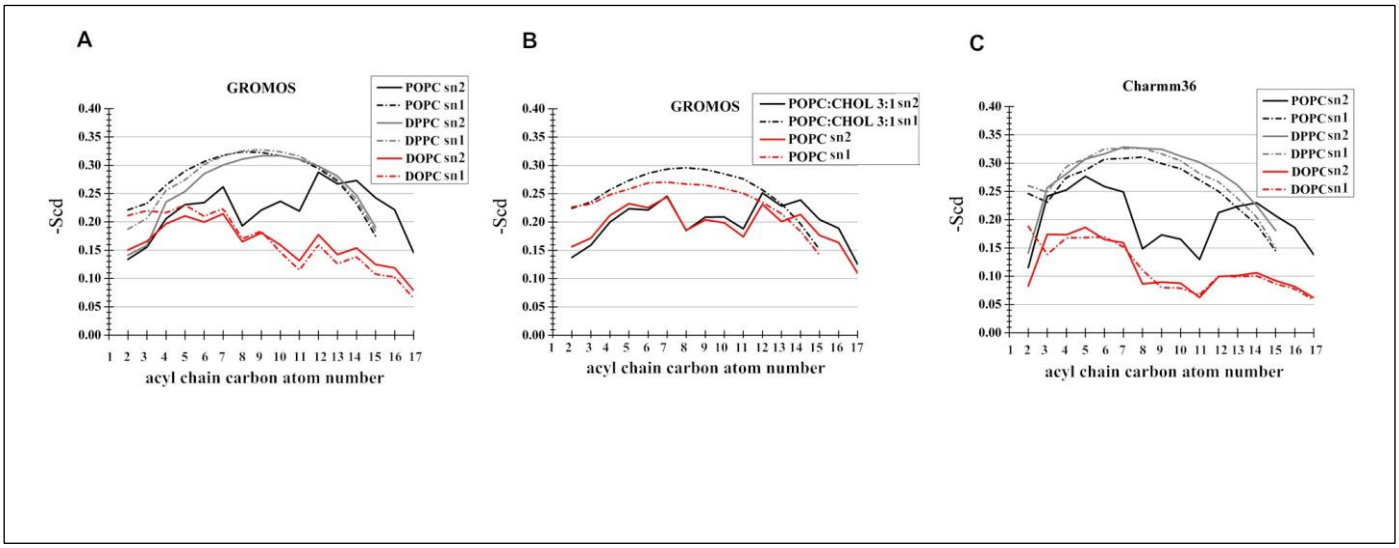

Figure 2

Lipid acyl chain order of the lipid bilayers used in this study. The order is represented by the deuterium order parameter, $-S_{CD}$, which is defined as $-S_{CD} = (1/2)S_z$, where $S_z = (1/2) \langle 3\cos^2(\theta_n) - 1 \rangle$, where θ_n stands for the angle between the vector linking n − 1 and n + 1 carbon atoms in the hydrocarbon chain and the bilayer normal, and the double angle bracket denotes the ensemble average. S_z can vary between 1 (full order along the normal) and –0.5 (full order perpendicular to the normal), which correspond to $-S_{CD} = 0.5$ and –0.25 , respectively. (A) Results on *sn1* and *sn2* chains of DOPC molecules in the r = 2.0 nm runs of the Gr-Ile$_{21}$-dopc system (#1), shown with red lines. Also shown (with black and grey lines) are the result of the acyl chains of POPC and of DPPC in the r = 2.0 nm runs of the Gr-Ile$_{21}$-1-1-1 system (#2). (B) Similar to (A) but the results on POPC molecules in the Gr-Ile$_{21}$-popc system (#4), and those in the Gr-Ile$_{21}$-3-1 system (#5) are shown. (C) Similar to (A) but results on DOPC in the Ch-Ile$_{21}$-dopc system (#8) and POPC and DPPC in the Ch-Ile$_{21}$-1-1-1 system (#9) are shown.

The obtained free energy profiles showed marked differences among bilayers, demonstrating weak attractive interhelical forces for the 1:1:1 bilayer, but largely repulsive forces in the DOPC bilayer for the range critical for the dimerization energy (from 1.3 to 1.5 nm) (Figure 3A). The 2:1:1 POPC/DPPC/cholesterol bilayer that had a

lower concentration of DPPC/cholesterol relative to the 1:1:1 bilayer exhibited a profile similar to the 1:1:1 bilayer (Figure 3A).

Table 1 Simulations and main results

ID (#)	system	constituents	simulation time[a]	ΔG^{dim} (± SE) (kJ/mol)	mean (± SE) of $\{V^{LJ}_{lipid\text{-}pept}(1.3) - V^{LJ}_{lipid\text{-}pept}(2.0)\}$ (kJ/mol)	mean (± SE) of $\{V^{Coul}_{lipid\text{-}pept}(1.3) - V^{Coul}_{lipid\text{-}pept}(2.0)\}$ (kJ/mol)
1	Gr-Ile$_{21}$-dopc	56 DOPC/2047 water	8×500ns×10	0.23 ± 0.56	136.2 ± 15.4	83.3 ± 11.6
2	Gr-Ile$_{21}$-1-1-1[b]	24 POPC/24 DPPC/24 chol/1835 water[c]	8×500ns×10	−1.34 ± 0.44	119.1 ± 3.9	17.4 ± 19.0
3	Gr-Ile$_{21}$-2-1-1	32 POPC/16 DPPC/16 chol/1835 water[c]	8×500ns×10	−1.22 ± 0.45	119.0 ± 8.8	12.2 ± 20.9
4	Gr-Ile$_{21}$-popc	56 POPC/1582 water	8×500ns×10	−0.06 ± 0.69	138.9 ± 17.5	65.2 ± 16.7
5	Gr-Ile$_{21}$-3-1	48 POPC/16 chol /1582 water[c]	8×500ns×10	−0.17 ± 0.75	133.5 ± 8.1	3.0 ± 21.9
6	Gr-IV-dopc	56 DOPC/1568 water	8×500ns×10	0.42 ± 0.59	114.5 ± 6.0	61.1 ± 12.4
7	Gr-IV-1-1-1	24 POPC/24 DPPC/24 chol/1835 water[c]	8×500ns×10	−1.81 ± 0.57	84.6 ± 8.7	−5.0 ± 11.4
	system	constituents	simulation time[a]	ΔG^{dim} (± SE) (kJ/mol)	mean (± SE) of $\{V^{LJ}_{lipid\text{-}pept}(1.3) - V^{LJ}_{lipid\text{-}pept}(1.6)\}$ (kJ/mol)	mean (± SE) of $\{V^{Coul}_{lipid\text{-}pept}(1.3) - V^{Coul}_{lipid\text{-}pept}(1.6)\}$ (kJ/mol)
8	Ch-Ile$_{21}$-dopc	pretend 56 DOPC/2047 water	8×500ns×4	−1.75 ± 0.22	78.1 ± 8.1	−5.2 ± 6.9
9	Ch-Ile$_{21}$-1-1-1	24 POPC/24 DPPC/24 chol/1835[c]	8×500 ns×4	−2.99 ± 0.30	61.8 ± 7.0	−37.5 ± 8.0

[a] For the GROMOS sets, ten different windows were computed, and for the Charmm set (#9) four windows covering 1.3-1.6 nm were computed. [b] Besides the runs listed here, eight 500ns runs with restraint of r =2.5 nm using a 1:1:1 bilayer (48 POPC/48 DPPC/48 cholesterol molecules and an approximate size of 6. 0×6.0 nm) were performed. [c] 'chol' stands for cholesterol

When we compared the POPC bilayer with the 3:1 POPC/cholesterol bilayer (#4 and #5 in Table 1), the dimer of $(Ile)_{21}$ was modestly stabilized in the 3:1 bilayer relative to the POPC bilayer (Figure 3A). The POPC bilayer also showed $(Ile)_{21}$ dimer stability largely similar to the DOPC bilayer (#1 and 4; Figure 3). Overall, the dimerization propensity of the $(Ile)_{21}$ peptide based on ΔG^{dim} showed a difference in the order of 1:1:1 > 2:1:1 > 3:1 POPC/cholesterol > POPC ≅ DOPC, which is in accordance with the order in the lipid acyl chain order (Table 1). Overall, the straightened (ordered) acyl chain-induced dimer stabilization is likely to occur for bilayers with a fairly wide range of order

parameter.

Although computational burden limited us to a short range analysis (r = 1.3 to 1.6 nm), the Charmm systems (#8 and #9) showed a similar trend of stabilization of the $(Ile)_{21}$ peptide dimer in the raft-like 1:1:1 relative to the DOPC bilayer (Figure 3B and Table 1). Stabilization of the helix dimer in the raft-like bilayer was also seen for the GROMOS system using the $I(VI)_{10}$ peptide that had alternating Ile and Val residues (Figure 3C).

To better address the possible artifacts due to the limited r range (i.e., $r \leq 2.0$ nm), we added eight 500 ns runs with a restraint of r =2.5 nm using a 1:1:1 bilayer (as commented in the footnote of Table 1). However, this set resulted in a mean force of ~–1.46 (± SE of 0.88) kJ/mol/nm, resulting in a flat extension of g(r) profile. So, although further analyses are necessary to rule out the possibility that long-range dynamics of the peptide self-association shows significant membrane dependency, it is unlikely that an extension of the range beyond 2.0 nm causes significant influences on the conclusion of this study. Overall, our simulations support the view that a bilayer with a high lipid-order parameter tends to stabilize the dimeric state of the peptides in a sequence-nonspecific manner. These findings reinforced our notion that PMF computation with UA and AA simulations on a scale of ~50 μs can be used to discuss the effects of lipid composition on the peptide dimerization energy to a resolution of ~1 kJ/mol [21].

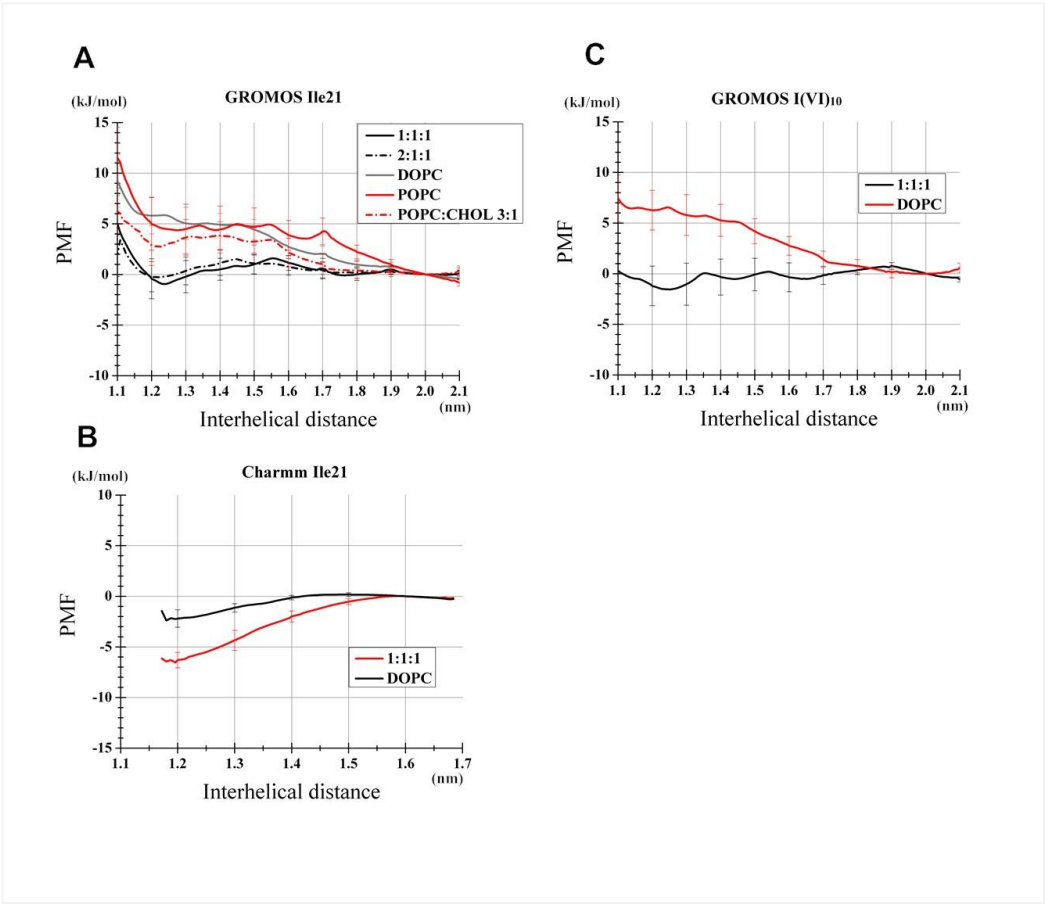

Figure 3 PMF profiles for TM helices dimerization. The PMF values relative to the value at r = 2.0 nm (GROMOS sets) or r = 1.6 nm (Charmm sets) is shown. (A) Results for the Gr-Ile$_{21}$-dopc (#1 of Table 1), and the raft-like Gr-Ile$_{21}$-1-1-1 (#2) and Gr-Ile$_{21}$-2-1-1 (#3) sets, Gr-Ile$_{21}$-popc (#4) and Gr-Ile$_{21}$-3-1 (#5) sets. Error bars represent SEs from the eight independent umbrella analysis sets. (B) Results for Ch-Ile$_{21}$-dopc (#8) and Ch-Ile$_{21}$-1-1-1 (#9) sets. (C) Results for Gr-IV-dopc (#6) and Gr-IV-1-1-1 (#7).

3.2 Transmembrane peptides were in direct contact with phospholipids but not with cholesterol in raft-like bilayer simulations

Neither of the raft-like bilayers (1:1:1 nor 2:1:1) spontaneously demixed into distinct domains in our analysis; both stayed as L_o phase, in accord with the simulations by

Niemelä et al that used sphingomyelin-containing bilayers [31] and the experiments [32]. Nonetheless, when the two-dimensional radial distribution functions (rdfs) were computed for the 1:1:1 bilayer with the dimerized $(Ile)_{21}$ peptides (r = 1.3 nm), cholesterol was nearly absent in the close vicinity (< 2.4 Å) of the peptides (*red line*, Figure 4A,B), with POPC and DPPC mainly solvating the peptides. The results with monomeric peptides (r = 2.0 nm) were similar to those with dimeric peptides (Figure 4C,D). Similar analysis on the POPC (#4) and 3:1 POPC/cholesterol (#5) systems also showed absence of cholesterol in the vicinity of peptides (Figure 4E,F,G,H). Thus, the peptides were mostly solvated by phospholipids but not by cholesterol in our raft-like bilayers. This can be explained by preferential association of cholesterol with phospholipids (especially with DPPC and POPC in our cases), which acts to exclude peptides from cholesterol-rich subareas.

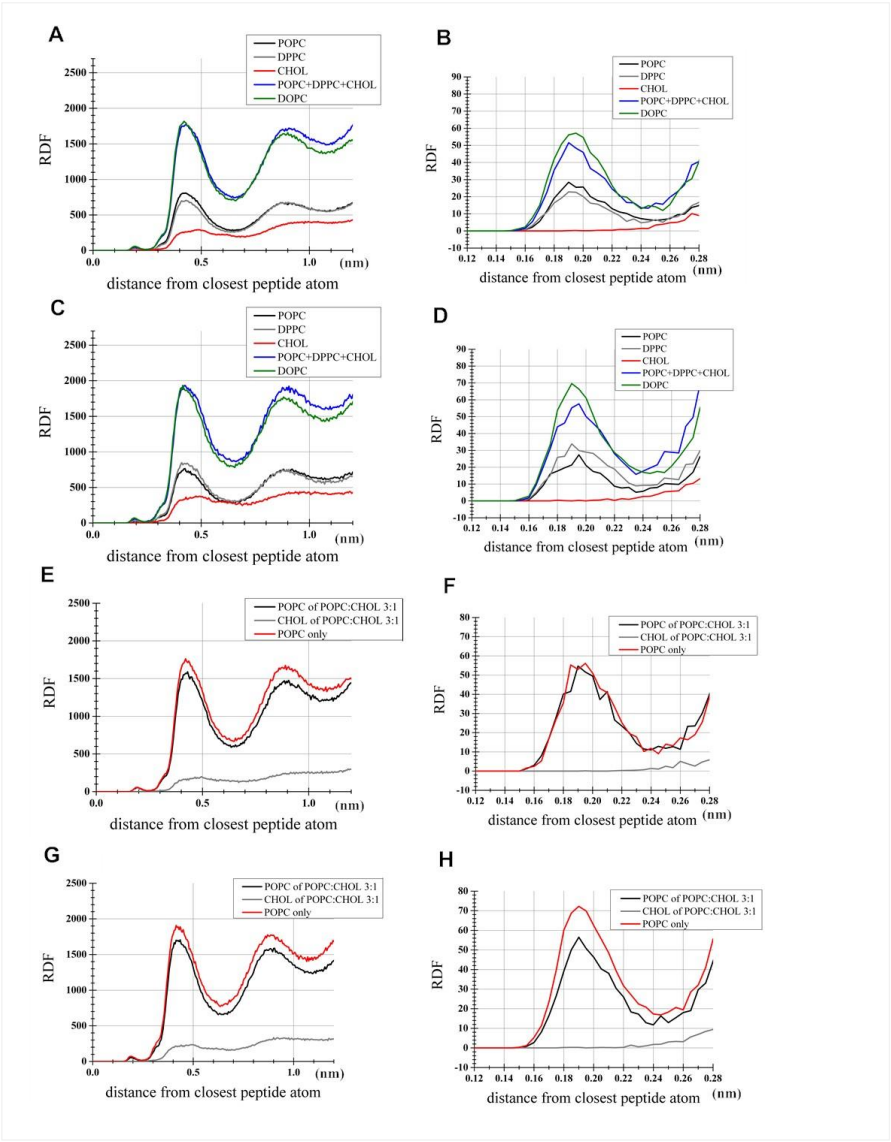

Figure 4

Two-dimensional radial distribution function (rdf) analysis of lipids around the peptides. Shown are the unnormalized density profile of lipid atoms residing at indicated distances from the nearest atom of the peptides. (A) The profile of DOPC (green line) in the Gr-Ile$_{21}$-dopc set (#1) and the profiles of POPC (black line), DPPC (grey line) and cholesterol (red line) in the Gr-Ile$_{21}$-1-1-1 set (#2). The umbrella simulations performed with the r = 1.3 nm constraints were analyzed. A blue line represents the sum of POPC, DPPC and cholesterol densities. (B) Similar to (A), but the proximal (near) range (< 0.28 nm) is highlighted with the expanded x- and y-axes. (C) Similar to (A) but the umbrella runs with r = 2.0 nm were used to analyze the monomeric state. (D) The near range of (C). (E) The profile of POPC (red line) in the Gr-Ile$_{21}$-popc runs (#4) and the profiles of POPC (black) and cholesterol (grey) in the Gr-Ile$_{21}$-3-1 runs (#5). The runs with r = 1.3 nm (dimeric state) were analyzed. (F) The near range of (E). (G) Results of the Gr-Ile$_{21}$-popc and Gr-Ile$_{21}$-3-1 sets with r = 2.0 nm. (H) The near range of (G).

3.3 Cholesterol and saturated FA modulate the lipid-peptide interaction potential energy to the degrees differing between monomeric and dimeric states, stabilizing peptide dimer in raft-like bilayers

To gain structural insights into the stabilization of peptide dimers in the raft-like bilayer simulations (Figure 3), the potential energy terms between the two peptides ($V_{pept\text{-}pept}$), between lipid molecules ($V_{lipid\text{-}lipid}$), and between peptides and lipid molecules ($V_{lipid\text{-}pept}$) were computed from the trajectories obtained in the umbrella sampling analysis using the procedure previously described in Castillo et al [29]. Given the local inhomogeneity of lipids seen in Figure 4, we initially hypothesized that the peptide dimers were stabilized in the raft-like bilayers by the exclusion of peptides from cholesterol-rich subareas due to the tight cholesterol-phospholipid interactions. If this 'exclusion-based scenario' is important, the lipid-lipid interaction component ($V_{lipid\text{-}lipid}$) of the total potential energy would give a clue as the peptide dimerization is always accompanied by increased lipid-lipid interactions. Indeed, $V_{lipid\text{-}lipid}$ decreased (reflecting increased lipid-lipid interaction) upon the peptide dimerization for all sets as shown by $V_{lipid\text{-}lipid}(1.3) < V_{lipid\text{-}lipid}(2.0)$ (Figure 5A,C and data not shown). However, the $V_{lipid\text{-}lipid}(r)$ drop upon dimerization was largely similar between the raft-like sets (the 1:1:1 and 2:1:1 sets) and the DOPC set, or rather greater in the DOPC set relative to the raft-like set (Figure 5C). So, our data did not support the idea that $V_{lipid\text{-}lipid}(r)$ contributes to the helix dimer stabilization in the 1:1:1 bilayer relative to the DOPC bilayer. Similarly, although a $V_{pept\text{-}pept}(r)$ profile drop was observed upon peptide dimerization (i.e., $V_{pept\text{-}pept}(1.3) < V_{pept\text{-}pept}(2.0)$), this drop was largely similar between the DOPC (#1) and the raft-like systems (#2 and 3) (Figure 5B,D), arguing against the role for this term in the helix dimer stabilization in the raft-like bilayers. The results for the Charmm sets also did not support the role of $V_{lipid\text{-}lipid}(r)$ or $V_{pept\text{-}pept}(r)$ in the helix stability in the raft-like bilayers (Figure 5E,F).

For the lipid-peptide term ($V_{lipid\text{-}pept}(r)$) of the potential energy, the value at r = 1.3 nm was always greater than at 2.0 nm, $V_{lipid\text{-}pept}(1.3) > V_{lipid\text{-}pept}(2.0)$, which normally occurred as some lipids were excluded from dimerized peptides and such lipids had less optimal contacts to peptides ('cost for desolvation') (Figure 6A,D). Importantly, the differential $\{V_{lipid\text{-}pept}(1.3) - V_{lipid\text{-}pept}(2.0)\}$ was small in the raft-like bilayers (#2 and #3) compared to the DOPC bilayer (#1), indicating that the energy cost for the desolvation upon the peptide dimerization was relatively small in the raft-like bilayers (Table 1, Figure 6A,D). Further decomposition of $V_{lipid\text{-}pept}(r)$ into the electrostatic energy term ($V^{Coul}_{lipid\text{-}pept}(r)$) and the LJ energy term ($V^{LJ}_{lipid\text{-}pept}(r)$) showed, for both the GROMOS $(Ile)_{21}$ and $I(VI)_{10}$ sets, that both terms were important; that is, both $\{V^{Coul}_{lipid\text{-}pept}(1.3) - V^{Coul}_{lipid\text{-}pept}(2.0)\}$

and $\{V^{LJ}_{lipid\text{-}pept}(1.3) - V^{LJ}_{lipid\text{-}pept}(2.0)\}$ had a difference in the order of the raft-like systems < the DOPC system (Table 1, Figure 6B,C,E,F). This indicates that both the electrostatic and the LJ potential energy interactions between lipids and peptides contributed to the helix dimer stabilization in the raft-like bilayers relative to the non-raft bilayer. The Charmm systems showed a similar trends (Figure 7D,E,F and data not shown). The POPC (#4) and the 3:1 POPC/cholesterol (#5) systems show an appreciable level of the bilayer dependency of $\{V^{Coul}_{lipid\text{-}pept}(1.3) - V^{Coul}_{lipid\text{-}pept}(2.0)\}$ but not of $\{V^{LJ}_{lipid\text{-}pept}(1.3) - V^{LJ}_{lipid\text{-}pept}(2.0)\}$, likely because of the relatively small difference in the acyl chain order between these systems (Table 1, Figure 7A,B,C and data not shown). Overall, these results suggest that the stabilization of the helix dimer in the raft-like bilayers relative to the non-raft bilayers was at least partly driven by the lipid-peptide term of the electrostatic as well as the LJ potential energy.

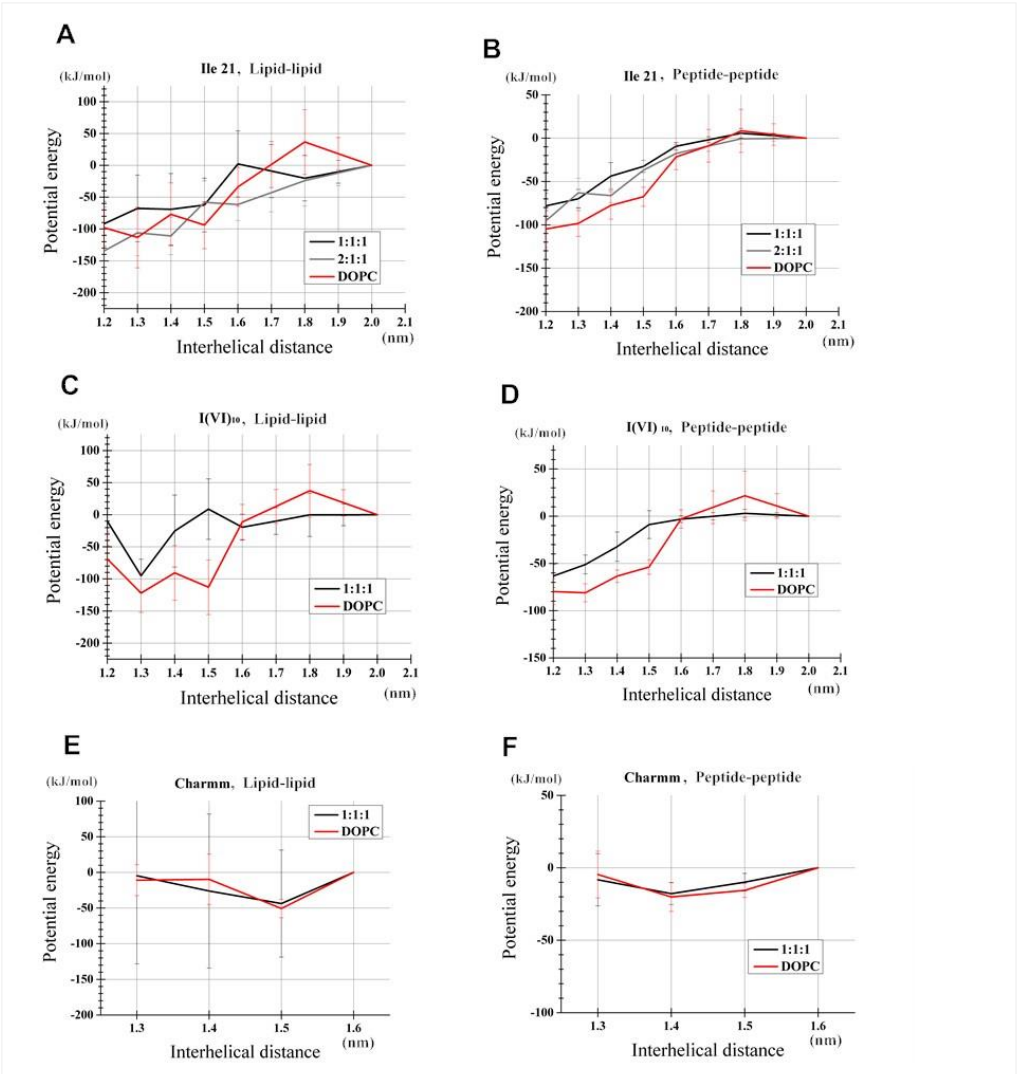

Figure 5

Supplementary data of the potential energy decomposition analysis. This figure shows potential energies relative to the values at r = 2.0 (the GROMOS systems) or 1.6 nm (the Charmm systems). (A) The lipid-lipid potential energy profile $V_{lipid\text{-}lipid}$ computed from the Gr-Ile$_{21}$-dopc (#1), the Gr-Ile$_{21}$-1-1-1 (#2) and the Gr-Ile$_{21}$-2-1-1 (#3) simulations. (B) The peptide-peptide potential energy profile $V_{pept\text{-}pept}$ computed for the sets analyzed in (A). (C) $V_{lipid\text{-}lipid}$ computed from the Gr-VI-dopc (#7), the Gr-VI-1-1-1 (#6). (D) The peptide-peptide potential energy profile $V_{pept\text{-}pept}$ computed for the sets analyzed in (C). (E) $V_{lipid\text{-}lipid}$ of the Ch-Ile$_{21}$-dopc (#8) and Ch-Ile$_{21}$-1-1-1 (#9) simulations. (F) $V_{pept\text{-}pept}$ computed for the simulations analyzed in (E).

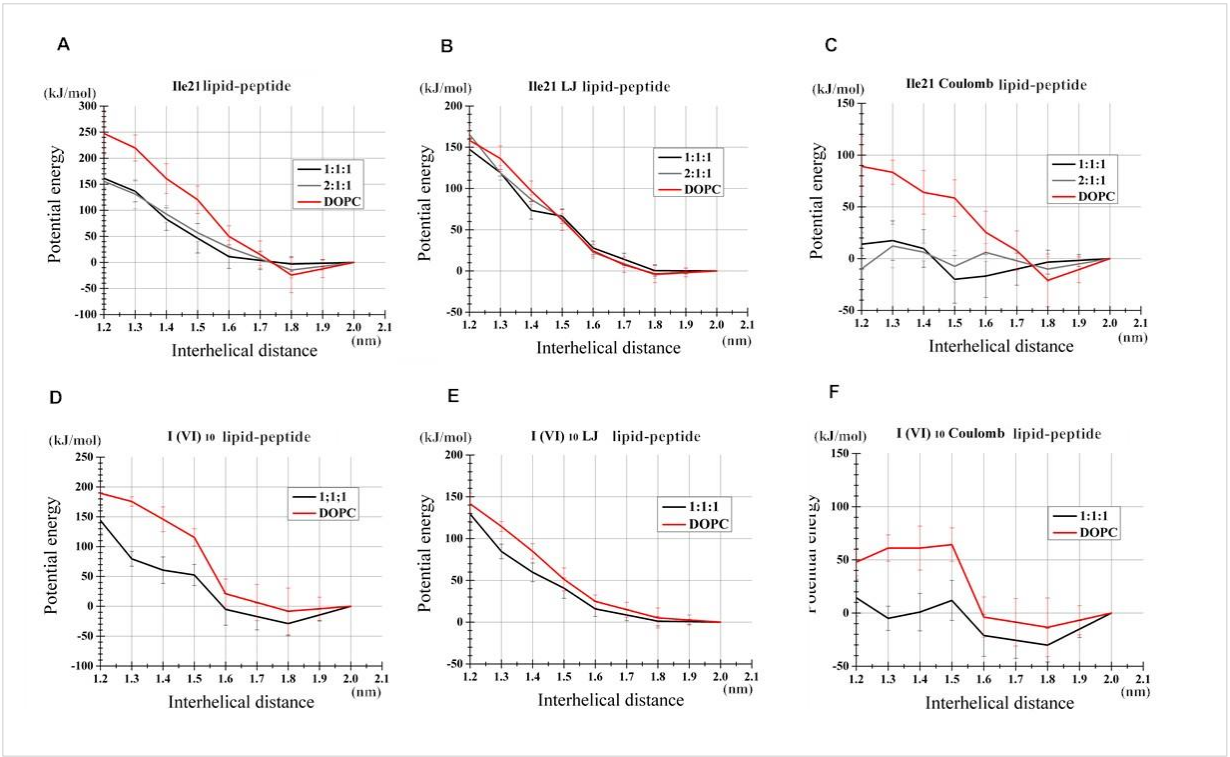

Figure 6 Decomposition analysis of the potential energy (i.e., Coulombic and LJ energies). The profile of the lipid-peptide term ($V_{lipid\text{-}pept}$) and the profiles of its LJ and Coulombic components $V^{LJ}_{lipid\text{-}pept}$ and $V^{Coul}_{lipid\text{-}pept}$ are shown. The simulations used for the PMF analysis were analyzed. The potential energies relative to the value at r = 2.0 nm are shown. (A-C) Results from the Gr-Ile_{21}-dopc (#1), the Gr-Ile_{21}-1-1-1 (#2), and the Gr-Ile_{21}-2-1-1 (#3) systems. (A) $V_{lipid\text{-}pept}$, i.e., the total lipid-peptide potential energy profile. (B) $V^{LJ}_{lipid\text{-}pept}$, i.e., the LJ component of (A). (C) $V^{Coul}_{lipid\text{-}pept}$, i.e., the Coulombic component of (A). (D-F) Results for the Gr-IV-dopc (#6) and the Gr-IV-1-1-1 (#7) systems. (D) $V_{lipid\text{-}pept}$, i.e., the total lipid-peptide potential energy profile. (E) $V^{LJ}_{lipid\text{-}pept}$. (F) $V^{Coul}_{lipid\text{-}pept}$.

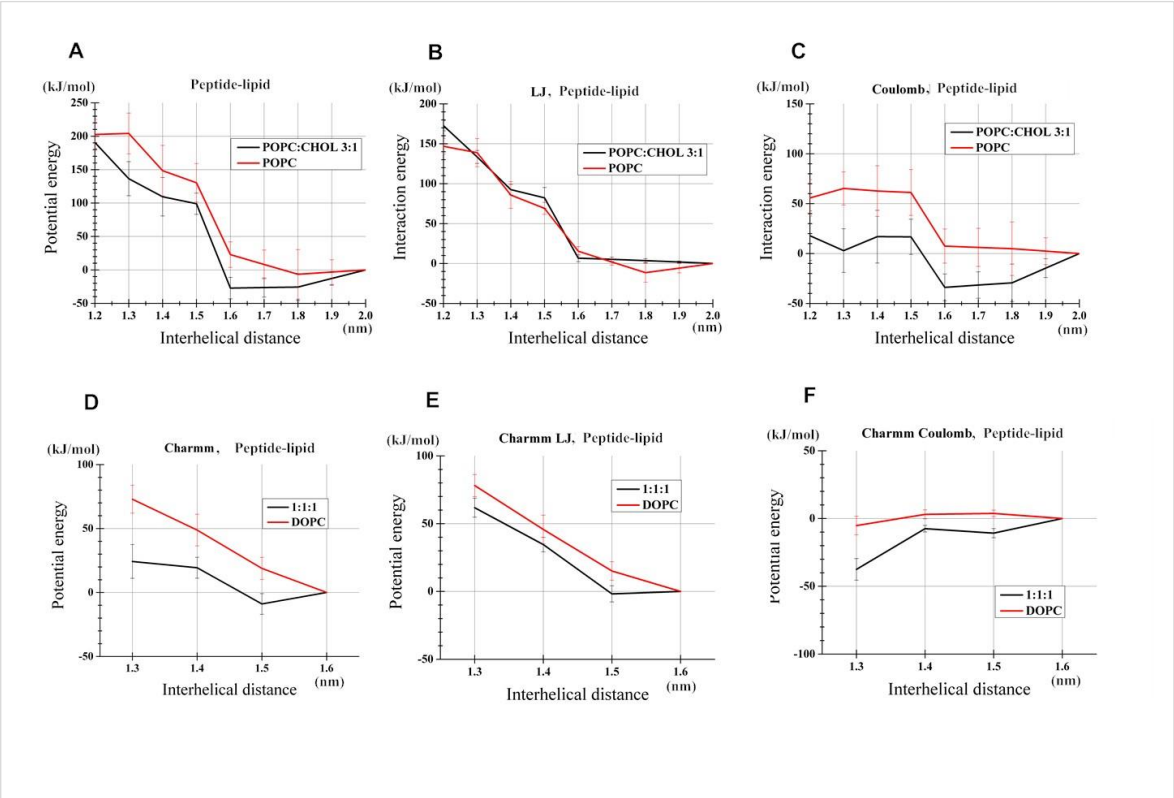

Figure 7

Decomposition analysis of the lipid-peptide potential energy. This figure shows potential energies relative to the values at r = 2.0 (the GROMOS systems) or 1.6 nm (the Charmm systems). (A) Profiles of $V_{lipid\text{-}pept}$ the lipid-peptide potential energy of the Gr-Ile_{21}-popc system (#4) and the Gr-Ile_{21}-3-1 system (#5). (B) Same as (A) but the profile for $V^{LJ}_{lipid\text{-}pept}$ is shown. (C) Same as (A) but the profile for $V^{Coul}_{lipid\text{-}pept}$ is shown. (D) Profiles of $V_{lipid\text{-}pept}$, the lipid-peptide potential energy of the Ch-Ile_{21}-dopc system (#8) and the Ch-Ile_{21}-1-1-1 system (#9). (E) Same as (D) but the profile for $V^{LJ}_{lipid\text{-}pept}$ is shown. (F) Same as (D) but the profile for $V^{Coul}_{lipid\text{-}pept}$ is shown.

Conclusion

In this report, we performed MD simulations to mainly measure the free energy for

self-association of model TM helical peptides. Overall, increases of cholesterol and saturated fatty acyl chains in the phospholipid bilayer tended to increase the dimerization propensity for both $(Ile)_{21}$ and $I(VI)_{10}$ model peptides. Contrary to our expectation that lipid-lipid interaction is strengthened by addition of cholesterol and acts to exclude the peptides from lipids and stabilize the peptide dimer, the profiles of the potential energy between lipid molecules did not support such "exclusion based scenario" (Figure 5). Rather, the profiles of the lipid-peptide potential energy exhibited the change suggestive of important roles for this term (Figure 6). In particular, the lipid-peptide electrostatic energy term showed profiles concordant with free energy profile. As the peptides used lacked the flanking polar/charged residues and the partial charges in the hydrocarbon chains were small (Charmm) or zero (GROMOS), the electrostatic interaction between lipid head groups atoms and peptide backbone atoms is likely to have significant impacts on the lipid mediated change in the monomer-dimer equilibrium of the peptides. In the companion paper [17], we compare the structural features in lipid-peptide contacts between the monomer and dimer states of the peptides as well as between the DOPC and the raft-like bilayers.

We would like to comment on a couple of technical issues. Together with our recent data, our findings show that independently-prepared eight initial structures and corresponding trajectories for each umbrella simulation set allow us to obtain good convergence of PMF profiles, and a reasonable level of convergence of potential energy profiles. On the other hand, we note several issues related with FFs. Compared with our previous data based on $(AALALAA)_3$ peptides [21] that showed dimerization energy of –5.2 and –9.9 kJ/mol for the GROMOS 53A6 and Charmm FF, respectively, the present study showed the free energy values closer to zero [Table 1]. In general, amino acid residues such as Gly and Ala tend to stabilize the helices dimer, likely through enabling closer positioning and increased electrostatic interaction between peptide backbones. In the present study, our use of the Ile-rich peptides would have weakened the dimerization propensity. Of technical importance, the use of GROMOS 53A6 in such analyses tends underestimate the peptide dimerization propensity, as our $(AALALAA)_3$ analysis has shown [21]. Our present choice of the GROMOS 53A6 parameters in the present study wsa based on the practical necessity to obtain convergence in reasonable computational cost. Intriguingly, particularly when embedded in helical peptides, Leu and Ala showed greater solvation energies in various apolar solvents and Leu and Ala-rich helices tended to smaller dimerization propensity, whereas Ile was relatively showed better results in such analyses compared to the cases with the Charmm FF [data not shown]. This led us to choose the Ile-rich peptides in this study. Nonetheless, a

substantial difference was observed in the dimerization energy between GROMOS 53A6 and Charmm FFs [Table 1], reinforcing the accuracy problem in utilization of UA FFs. As we discussed previously, even a slight degree of inaccuracy in solvation energy of amino acid side chains can lead to a substantial deviation in the TM dimerization energy, as the later energy integrates the inaccuracies associated with each amino acid residue along the peptides used [21]. Although we chose the standard GROMOS 53A6 set in this study, it is quite possible that future quantitative analyses based on UA FFs may be assisted by reparameterization of the LJ parameters between lipid atoms and peptides atoms guided by the reference values derived from an AA FF computation and/or experimental values [21].

Conflict of Interest Disclosure

The authors declare no competing financial interest.

References

(1) Sarabipour S. Parallels and Distinctions in FGFR, VEGFR, and EGFR Mechanisms of Transmembrane Signaling. Biochemistry. 2017;56:3159-3173.

(2) Williams LT. Signal transduction by the platelet-derived growth factor receptor. Science. 1989;243(4898):1564-1570.

(3) Schlessinger J. Signal transduction by allosteric receptor oligomerization. Trends Biochem Sci. 1988;13(11):443-447.

(4) Bocharov EV, Mineev KS, Pavlov KV, Akimov SA, Kuznetsov AS, Efremov RG, Arseniev AS. Helix-helix interactions in membrane domains of bitopic proteins: Specificity and role of lipid environment. Biochim Biophys Acta. 2017;1859:561-576.

(5) Belov AA, Mohammadi M. Molecular mechanisms of fibroblast growth factor signaling in physiology and pathology. Cold Spring Harb Perspect Biol. 2013;5(6): a015958.

(6) Hong H, Bowie JU. Dramatic destabilization of transmembrane helix interactions by features of natural membrane environments. J Am Chem Soc. 2011;133(29):11389-

11398.

(7) Murray DH, Tamm LK. Clustering of syntaxin-1A in model membranes is modulated by phosphatidylinositol 4,5-bisphosphate and cholesterol. Biochemistry. 2009;48(21):4617-4625.

(8) Smith SM, Lei Y, Liu J, Cahill ME, Hagen GM, et al. Luteinizing hormone receptors translocate to plasma membrane microdomains after binding of human chorionic gonadotropin. Endocrinology. 2006; 147:1789-1795.

(9) Płóciennikowska A, Hromada-Judycka A, Borzęcka K, Kwiatkowska K Co-operation of TLR4 and raft proteins in LPS-induced pro-inflammatory signaling. Cell Mol Life Sci. 2015; 72:557-581.

(10) Nishizawa M, Nishizawa K Cholesterol and saturated fatty acid stabilize dimerization of helical transmembrane peptides by lowering energy cost related to peptides desolvation from lipids upon dimerization: an insight from atomistic simulation. Biomed Res Clin Prac. 2017; 2:1-8.

(11) Anbazhagan V, Schneider D. The membrane environment modulates self-association of the human GpA TM domain--implications for membrane protein folding and transmembrane signaling. Biochim Biophys Acta. 2010;1798(10):1899-1907.

(12) Lange Y, Steck TL. Active membrane cholesterol as a physiological effector. Chem Phys Lipids. 2016;199:74-93.

(13) Fantini J, Barrantes FJ. How cholesterol interacts with membrane proteins: an exploration of cholesterol-binding sites including CRAC, CARC, and tilted domains. Front Physiol. 2013;4:31.

(14) Yano Y, Kondo K, Kitani R, Yamamoto A, Matsuzaki K. Cholesterol-induced lipophobic interaction between transmembrane helices using ensemble and single-molecule fluorescence resonance energy transfer. Biochemistry. 2015; 54(6):1371-1379.

(15) Yang ST, Kreutzberger, AJ, Lee J, Kiessling V, Tamm, LK The role of cholesterol in membrane fusion. Chem Phys Lipids. 2016; 199:136-143.

(16) Yano Y, Furukawa N, Ono S, Takeda Y, Matsuzaki K. Selective amine labeling of cell surface proteins guided by coiled-coil assembly. Biopolymers. 2016;106:484-490.

(17) Nishizawa M, Nishizawa K Sequence-nonspecific stabilization of transmembrane helical peptide dimer in lipid raft-like bilayers in atomistic simulations. II. Acyl chain order-associated changes in phospholipid-peptide coordination

(18) Hess B, Kutzner C, van der Spoel D, Lindahl E. GROMACS 4: Algorithms for Highly Efficient, Load-Balanced, and Scalable Molecular Simulation. J Chem Theory Comput. 2008; 4:435-447.

(19) Malde AK, Zuo L, Breeze M, Stroet M, Poger D, Nair PC, Oostenbrink C, Mark AE. An Automated force field Topology Builder (ATB) and repository: version 1.0. J

Chem Theory Comput. 2011; 7:4026-4037.

(20) Berendsen HJC, Postma JPM, van Gunsteren WF, Hermans J. Intermolecular forces, interaction models for water in relation to protein hydration. D. Reidel Publishing, Dordrecht, The Netherlands, 1981, 331-342.

(21) Nishizawa M, Nishizawa K Free energy of helical transmembrane peptide dimerization in OPLS-AA/Berger force field simulations: inaccuracy and implications for partner-specific Lennard-Jones parameters between peptides and lipids. Molecular Simulation. 2016; 42: 916-926.

(22) Nishizawa, M, Nishizawa, K Potential of mean force analysis of the self-association of leucine-rich transmembrane α-helices: difference between atomistic and coarse-grained simulations. J Chem Phys. 2014; 141(7): 08B610_1.

(23) Bjelkmar P, Larsson P, Cuendet MA, Hess B, Lindahl E. Implementation of the CHARMM Force Field in GROMACS: Analysis of Protein Stability Effects from Correction Maps, Virtual Interaction Sites, and Water Models. J Chem Theory Comput. 2010;6:459–466.

(24) Klauda JB, Venable RM, Freites JA, O'Connor JW, Tobias DJ, Mondragon-Ramirez C, Vorobyov I, MacKerell Jr. AD, Pastor RW. J Phys Chem B 2010;114:7830–7843.

(25) Darden T, York D, Pedersen L. Particle mesh Ewald: An N·log(N) method for Ewald sums in large systems J Chem Phys. 1993; 98:10089.

(26) Berendsen HJC, Postma JPM, van Gunsteren WF, DiNola A, Haak JR Molecular dynamics with coupling to an external bath. J Chem Phys. 1984; 81:3684-3690.

(27) Hess B, Bekker H, Berendsen HJC, et al. LINCS: a linear constraint solver for molecular simulations. J. Comput Chem. 1997;18:1463– 1472.

(28) Miyamoto S, Kollman PA. Settle: an analytical version of the SHAKE and RATTLE algorithm for rigid water models. J Comput Chem. 1992;13:952–962.

(29) Kumar S, Rosenberg JM, Bouzida D, Swendsen RH, Kollman PA. The weighted histogram analysis method for free-energy calculations on biomolecules. I. The method. J Comput Chem. 1992;13:1011–1021.

(30) Castillo N, Monticelli L, Barnoud J, Tieleman DP Free energy of WALP23 dimer association in DMPC, DPPC, and DOPC bilayers. Chem Phys Lipids. 2013; 169: 95-105.,

(31) Niemelä PS, Ollila S, Hyvönen MT, Karttunen M, Vattulainen I. Assessing the nature of lipid raft membranes. PLoS Comput Biol. 2007;3(2):e34.

(32) Veatch SL, Keller SL. Seeing spots: complex phase behavior in simple membranes. Biochim Biophys Acta. 2005;1746:172-185.